Noncontact measurement of nerve displacement during action potential with a dual-beam low-coherence interferometer

Christopher Fang-Yen and Mark C. Chu

G. R. Harrison Spectroscopy Laboratory, Massachusetts Institute of Technology, Cambridge, Massachusetts 02139

H. Sebastian Seung

Howard Hughes Medical Institute and Department of Brain and Cognitive Sciences, Massachusetts Institute of Technology, Cambridge, Massachusetts 02139

Ramachandra R. Dasari and Michael S. Feld

G. R. Harrison Spectroscopy Laboratory, Massachusetts Institute of Technology, Cambridge, Massachusetts 02139

Received March 17, 2004

We have used a novel phase-referenced heterodyne dual-beam low-coherence interferometer to perform what we believe are the first noncontact measurements of surface motion in a nerve bundle during the action potential. Nerve displacements of ~5-nm amplitude and ~10-ms duration are measured without signal averaging. This interferometer may find general application in measurement of small motion in cells and other weakly scattering samples. © 2004 Optical Society of America

OCIS codes: 120.3180, 170.3880.

Nerve fibers exhibit rapid outward lateral surface displacements during the action potential. This swelling phenomenon, which is generally attributed to water influx into axons, has been observed in a number of invertebrate and vertebrate preparations.[1,2]

Observations of nerve swelling have so far employed sensors placed in physical contact with the nerve, which may introduce artifacts. We describe here a novel dual-beam heterodyne low-coherence interferometer and its application to optically measuring the swelling effect in a lobster nerve bundle. Earlier studies of nerve changes by use of interferometry are described in Refs. 3 and 4.

Measurement of nerve displacements requires a system that is capable of measuring nanometer-scale displacements in surfaces of low reflectivity at ~1-kHz bandwidth. Laser Doppler vibrometry,[5] speckle vibrometry,[6] and laser feedback interferometry[7] are sensitive to small displacements but are susceptible to external perturbations and may be difficult to apply to weakly reflecting objects.

The interferometer design described here is based on phase-referenced interferometry,[8] in which phase noise is canceled by measurement of motions relative to a nearby surface. An unequal-arm Michelson interferometer compensates for the path delay between sample and reference reflections, and a differential measurement scheme that uses a passive reference gap compensates for phase noise in the Michelson interferometer. The use of low-coherence (broadband) light permits depth-selective measurement of weak reflections, as in optical coherence tomography.[9]

The interferometer design incorporates both fiber and free-space elements (Fig. 1). Light from a fiber-coupled superluminescent diode (Optospeed; center wavelength 1550 nm, FWHM bandwidth, 35 nm) is

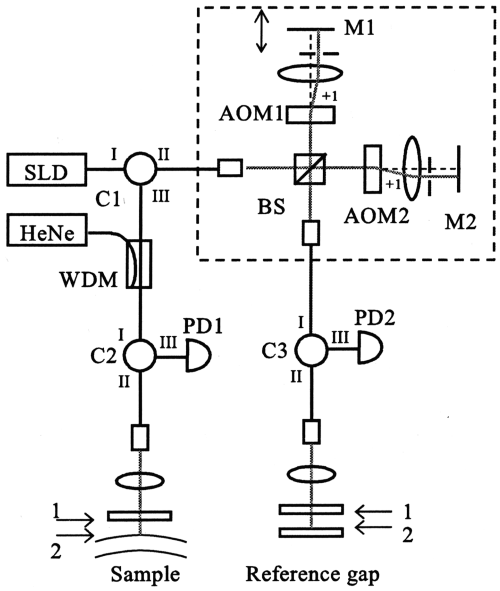

Fig. 1. Interferometer design. Dashed box, Michelson interferometer. SLD, superluminescent diode; AOM1, AOM2, acousto-optic modulators; M1, M2, mirrors; C1–C3, optical circulators; BS, beam splitter; PD1, PD2, InGaAs photodetectors; HeNe, guide laser; WDM, wavelength-division multiplexer; 1's and 2's, surfaces of the sample and of the reference gap, described in text.

0146-9592/04/172028-03$15.00/0

collimated and enters a Michelson interferometer containing acousto-optic modulators (Brimrose TEF-110) driven at frequencies of $\omega_1 = 110.1$ MHz and $\omega_2 = 110$ MHz. The difference in double-pass frequency shift between the two arms is $\Omega = 2(\omega_1 - \omega_2) = 200$ kHz. A mirror mounted upon a translation stage allows control of round-trip optical path difference ΔL between the two interferometer arms. Light enters and exits the Michelson interferometer through the fiber-optic collimators.

The output from each of the two ports of the Michelson interferometer is a dual beam composed of two low-coherence fields with different frequency shifts and a variable delay. One of the dual beams is incident onto the nerve chamber setup (detailed in Fig. 2); the other, onto a reference gap. The nerve setup and the reference gap each contain two reflective surfaces separated by an adjustable distance and are aligned to reflect the incident light back to its respective fiber. All but one of these surfaces are interfaces between air and uncoated glass. In the sample the second reflection comes from the interface between the nerve surface and air.

Let ΔL_S and ΔL_R be the round-trip optical path length differences between reflections from surfaces 1 and 2 of the sample and of the reference gaps, respectively. The various components are adjusted such that path lengths ΔL, ΔL_S, and ΔL_R are all equal within the source coherence length. When this condition is satisfied the ac-coupled photodetectors (New Focus 2011) record heterodyne signals $V_1(t) = V_1{}^0 \cos[\Omega t - \phi_1(t)]$, $V_2(t) = V_2{}^0 \cos[\Omega t - \phi_2(t)]$ because of interference between (1) light that traverses arm 1 of the Michelson interferometer and reflects from surface 2 of the sample (or reference gap) and (2) light that traverses arm 2 of the Michelson interferometer and reflects from surface 1 of the sample (or reference gap). The phase difference between the two heterodyne signals (up to a multiple of 2π) is $\Delta\phi(t) = \phi_1(t) - \phi_2(t) = k_0[(\Delta L_S - \Delta L) - (\Delta L_R - \Delta L)] = k_0(\Delta L_S - \Delta L_R)$, where k_0 is the central wave number of the source. Note that the quantity most susceptible to phase noise, Michelson path delay ΔL, is canceled in this differential measurement scheme.

Polarization-independent optical circulators are used to maximize detected power and keep reflected light from reentering the Michelson interferometer. A looped-fiber polarization controller (not shown) placed after the superluminescent diode is used to minimize effects of polarization-mode dispersion in the fiber components.

Photodetector outputs $V_1(t)$ and $V_2(t)$ are digitized by a 12-bit analog-to-digital card (National Instruments PCI-6110) at a rate of 5 Msamples/s. A computer program calculates the phase difference through $\Delta\phi(t) = \arg(\{V_2(t) + iH[V_2(t)]\}/\{V_1(t) + iH[V_1(t)]\})$, where H is the Hilbert transform. The phase shift is expressed as relative surface displacement $\Delta d(t) = \Delta\phi(t)/2k_0$ and is low-pass filtered.

To verify that the interferometer performs an accurate displacement measurement, we used as a sample a planar Fabry–Perot cavity with cavity spacing sinusoidally modulated at 300-Hz frequency and 27-nm amplitude by a piezoelectric transducer. Dual-beam measurements of amplitude and frequency were in good agreement with values determined by monitoring the transmission of a 632.8-nm helium–neon laser beam.

To assess the noise performance of the interferometer we aligned a glass coverslip such that the two sides of the glass reflected the light back to the fiber collimator. A test measurement at 1-kHz bandwidth gave a rms phase noise of 0.069 mrad, corresponding to a rms displacement of 8.5 pm.

For the data shown in this paper, the walking leg nerve (~1-mm diameter, ~50-mm length) from an American lobster (*Homarus americanus*) was dissected and placed in an acrylic nerve chamber (Fig. 2). The chamber contains five wells filled with a saline solution.[10] Between wells the nerve is surrounded by an insulating layer of petroleum jelly to maximize interwell resistance. A compound action potential is generated by a current pulse from a stimulus isolator and is detected at the other end by an amplifier with gain of 10^4. In the central well the nerve rests upon a small glass platform such that it is not submerged in the saline solution. The light power incident upon the nerve was approximately 80 μW. The amplitude of the heterodyne signal recorded at the photodetector corresponds to an ~1-μW modulation.

Figure 3 shows the electrical potential and optically measured displacement of a nerve for one trial. The spike at time zero in the electrical signal is due to a stimulus artifact. It is followed by a series of peaks that correspond to action potentials of axons in the nerve bundle. The optical signal shows a peak height of ≈5 nm and a FWHM duration of ≈10 ms, with a direction corresponding to an upward displacement. The noise of the displacement measurement was $\sigma \approx 0.25$ nm for 1-kHz bandwidth. The displacements were observed in approximately half of the nerve preparations and varied in amplitude from 0 to 8 nm for 5-mA, 1-ms stimulation.

To control for artifacts such as thermal expansion we measured the peak electrical and displacement

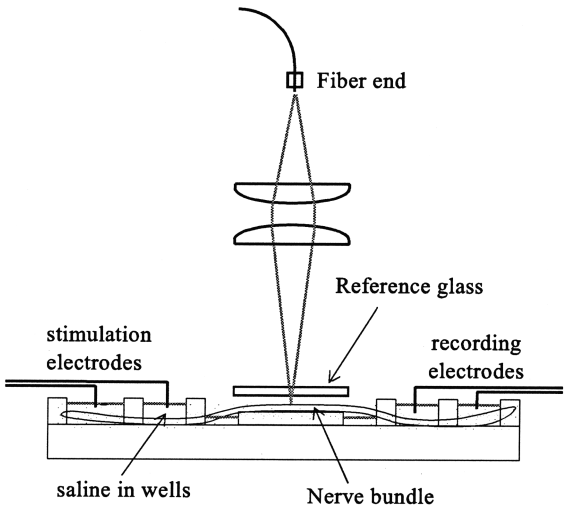

Fig. 2. Nerve chamber setup.

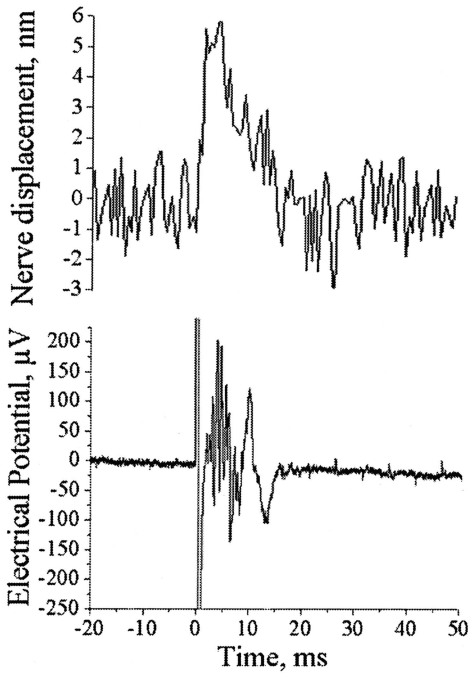

Fig. 3. Nerve displacement and electrical potential. Single-shot measurements (no signal averaging). Stimulus current for this trial, 4 mA. Displacement signal low-pass filtered at 1 kHz. Positive displacements correspond to an increase in the height of the nerve surface. A linear component with a negative slope of ~300 nm/s, which most likely was due to nerve drying, was subtracted from the displacement signal.

signals of one nerve as a function of stimulus current (Fig. 4). The electrical and displacement signals exhibited nearly identical threshold currents (≈1.5 mA) and saturation currents (≈5 mA), strongly suggesting that the displacements are due to action potentials.

The dual-beam low-coherence interferometer may have many applications in measuring nanometer-scale motions of living cells. We are developing a microscope based on this interferometer to detect mechanical changes in single neurons during the action potential. Such motions are of fundamental interest[11] and may lead to new techniques for intrinsic neuroimaging.

This research was supported by National Institutes of Health grant P41-RR02594-18 and by the Hamamatsu Corporation. The authors thank David Kleinfeld for many helpful suggestions. C. Fang-Yen's e-mail address is minwah@mit.edu.

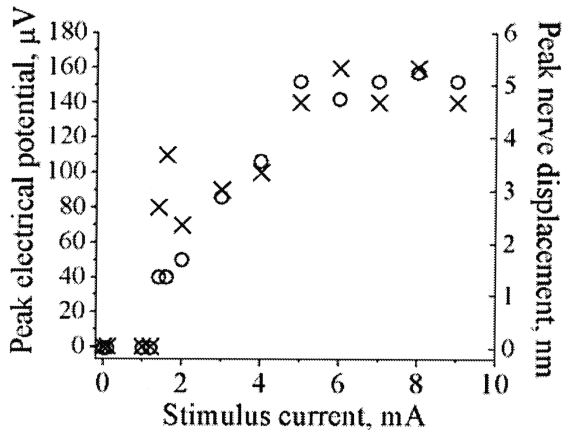

Fig. 4. Peak electrical potential (crosses) and nerve displacements (circles) for a single nerve, with variable-stimulus current amplitude. Data in Figs. 3 and 4 are not from the same nerve.

References

1. K. Iwasa, I. Tasaki, and R. C. Gibbons, Science **210,** 338 (1980).
2. I. Tasaki, Physiol. Chem. Phys. Med. NMR **20,** 251 (1998).
3. R. Sandlin, L. Lerman, W. Barry, and I. Tasaki, Nature **217,** 575 (1968).
4. D. Kleinfeld and A. LaPorta, in *Light Scattering Imaging of Neural Tissue Function*, D. M. Rector and J. S. George, eds. (Humana, Totowa, N.J., to be published).
5. L. E. Drain, *The Laser Doppler Technique* (Wiley, New York, 1980).
6. P. K. Rastogi, *Digital Speckle Pattern Interferometry and Related Techniques* (Wiley, Chichester, U.K., 2001).
7. K. Otsuka, K. Abe, J. Ko, and T. Lim, Opt. Lett. **27,** 1339 (2002).
8. C. Yang, A. Wax, M. S. Hahn, K. Badizadegan, R. R. Dasari, and M. S. Feld, Opt. Lett. **26,** 1271 (2001).
9. D. Huang, E. A. Swanson, C. P. Lin, J. S. Schuman, W. G. Stinson, W. Chang, M. R. Hee, T. Flotte, K. Gregory, C. A. Puliafito, and J. G. Fujimoto, Science **254,** 1178 (1991).
10. A. Watanabe, J. Physiol. **389,** 223 (1987).
11. P. Zhang, A. M. Keleshian, and F. Sachs, Nature **413,** 428 (2001).